Acta Cryst. (1991). B47, 683–692

Determination of the Antimony Substitution Site in Calcium Fluorapatite from Powder X-ray Diffraction Data

BY BARRY G. DEBOER

GTE Electrical Products, 100 Endicott St, Danvers, Massachusetts 01923, USA

AND A. SAKTHIVEL,* J. R. CAGLE AND R. A. YOUNG

School of Physics, Georgia Institute of Technology, Atlanta, Georgia 30332, USA

(*Received* 8 *January* 1991; *accepted* 24 *April* 1991)

Abstract

Comparison of powder X-ray diffraction data from a 2·2 wt% antimony-substituted calcium fluorapatite [0·185 Sb atoms per unit cell containing $Ca_{10}F_2(PO_4)_6$] with data from an undoped sample shows electron density changes corresponding to antimony substitution at the Ca(2) (mirror) site. Many properties of this 2·2 wt% Sb sample indicate that it corresponds to commercial halophosphate phosphors of lower Sb concentration. Differing properties are shown by a 3·1 wt% Sb sample for which no diffraction evidence is found for substitution at the Ca(2) site, but for which electron density difference maps do suggest substitution at the Wyckoff 2(*c*) and 2(*d*) sites of $P6_3/m$, between Ca(1) (threefold) positions. Both Rietveld refinements and Fourier inversion of the differences between observed intensities were used to reach these conclusions.

1. Introduction

Apatitic halophosphate phosphors are the backbone of the fluorescent lighting industry, with worldwide consumption of the order of 10 tons per day. Their luminescence depends upon the incorporation of a small amount of antimony(III), but in spite of the approximately 40 years since their invention, the location of the antimony in the host crystal is not as certainly known as it might be. Its nearest-neighbor environment is yet more uncertain, undermining theoretical efforts to understand luminescence, excitation transfer and degradation mechanisms.

The most popular model, that of Ouweltjes (1952), has Sb^{3+} substituting for a Ca^{2+} adjacent to the halide chain, and charge compensated by substitution of an oxide for the adjacent halide ion. This model has been said to be supported by (at least) the input composition adjustments needed to manufacture good phosphor (Mitsuishi & Emoto, 1967), by chemical analyses of finished phosphor (Rabatin, Gillooly & Hunter, 1967), and by energy-level calculations fitting the excitation and emission spectra (Soules, Davis & Kreidler, 1971). However, room for doubt may be found in the importance of vapor-phase transport and losses in the synthesis (Rabatin & Gillooly, 1965), the low solubility of antimony in haloapatites, the possible and actual presence of small amounts of other phases (not necessarily crystalline or of known or definite composition), and uncertainties due to the breadth of the spectral bands. The lack of an unpaired electron on Sb^{III} eliminates a class of physical methods, and the nuclei do not give high sensitivity in nuclear-spin-dependent methods. A recent publication (Mishra, Patton, Dale & Das, 1987) fits the ^{121}Sb Mossbauer absorption spectrum with an $:SbO_3^{3-}$ model and infers substitution for PO_4^{3-}.

The ability of X-ray diffraction analysis to examine the three-dimensional electron density distribution in crystals gave promise of directly 'seeing' the location of high electron density ($Z = 51$) Sb in the presence of lighter host atoms ($Z = 20$, 15, 9, 8). Of course, the most desirable way to do this experiment would be to take diffraction data from a very heavily doped single crystal of fluorapatite. Use of the pure fluorapatite avoids known complications in mixed-halide systems as well as minimizing the non-antimony electron density. Unfortunately, appreciable antimony content seems to be attainable only in powders. Warren, Ryan, Hopkins & VanBroekhoven (1975) report only 0·036 wt% antimony in Czochralski-grown single crystals in spite of 'heroic measures'. On the other hand, we believed that powder diffraction measurement and whole-pattern (Rietveld) fitting methods had developed to the point of making the experiment on powder samples feasible. A simple estimate of the changes expected in the diffraction pattern due to the ~1 wt% antimony found in commercial phosphors indicates ~2% intensity changes, near the limit of the data-taking method's precision. Clearly, we require both the

* Present address: Hercules Inc., Edgemont Ave, Covington, Virginia 24426, USA.

0108-7681/91/050683-10$03.00

highest antimony substitution levels and the most precise diffraction data attainable. Very valuable guidance toward the preparation of suitable samples was found in a publication by Gillooly (1971) in which only refractory starting materials are used, including calcium meta-antimonate, $CaSb_2O_6$, as the antimony source. Preliminary accounts of this work have been given (Young, 1988; Young, DeBoer, Sakthivel & Cagle, 1988).

2. Sample preparation and characterization

All materials used were either ACS reagent grade or Sylvania luminescent grade (GTE Electrical Products, Towanda, PA). Calcium meta-antimonate, $CaSb_2O_6$, was prepared by firing wet-mixed $Ca(NO_3)_2$ and Sb_2O_3 at 1273 K in air, then driving off excess antimony oxides at 1473 K, as described in detail elsewhere (Young, Sakthivel & DeBoer, 1991).

High-antimony calcium fluorapatite was prepared by two routes. In the first, preformed undoped fluorapatite powder was fired with calcium meta-antimonate as the antimony source, plus small amounts of calcium pyrophosphate, $Ca_2P_2O_7$, and sometimes CaO and/or CaF_2, as various 'compensations for' the antimony were tried. The second route consisted of firing appropriate mixtures of powdered CaO, CaF_2, $Ca_2P_2O_7$ and $CaSb_2O_6$. Firing conditions were kept fixed as 2·5 h at 1473 K in covered Coors porcelain crucibles in air. A portion of the product was dissolved in 2·4 *M* HCl and analyzed for incorporated Sb^{3+} by permanganate titration. The titration method was checked against blanks of pure fluorapatite and against mixtures of fluorapatite and weighed amounts of Sb_2O_3, and found to agree with the theoretical titer of the $KMnO_4$ solution. Remaining unreacted meta-antimonate was determined by weighing the acid insoluble residue (confirmed to be the meta-antimonate by its X-ray diffraction pattern and previously found to be insoluble, even in boiling 6 *M* acid). Other phases were checked for in routine X-ray diffraction patterns; residual CaO is sensitively detected by the basic pH of a water slurry. Because the reaction is strongly influenced by vapor transport (Rabatin & Gillooly, 1965) and losses, various formulations were explored. The desired high levels of incorporated Sb were never obtained until firing ~10 g quantities was abandoned in favour of ~120 g charges. The exteriors of these larger fired cakes were always removed and discarded, as they were frequently discolored and dimly luminescent.

The level of Sb^{3+} incorporated into the fired products was measured in three different ways: by the permanganate titration, by the brightness of the luminescence of a flat plaque of the powder under a small mercury ultraviolet lamp, and by the height of a peak in the infrared spectrum at about 686 cm^{-1} measured on weighed samples in KBr pellets. The 686 cm^{-1} peak has previously been shown to correlate with Sb content in haloapatites (Dale, 1987; Davis, Kreidler, Parodi & Soules, 1971). These are plotted in Fig. 1 for all of the larger scale synthesis attempts. The values for a commercial 'blue halo', $Ca_{10}F_2(PO_4)_6$:Sb, Sylvania type 2440, are included for comparison. The scatter of the points in these plots is thought to be real, as the measurements are reasonably reproducible (see §5, below). In any case, (*a*) we seem to have the desired materials up to 2·13 wt% Sb and (*b*) something is different about the three samples clustered near 3 wt%. (Samples in both groups resulted from each of the two preparative routes.)

Samples selected for the diffraction study were the highest Sb content 'normal'-appearing sample of Fig. 1, designated hereinafter as the '2%Sb' sample, and one of the anomalous group, referred to as the '3%Sb' sample. The 2%Sb sample contained 2·14 wt% soluble Sb^{3+}, corresponding to 0·185 Sb atoms per unit cell of $Ca_{10}F_2(PO_4)_6$, after correction for the 2·23 wt% unreacted calcium meta-antimonate that is the only other detectable phase.

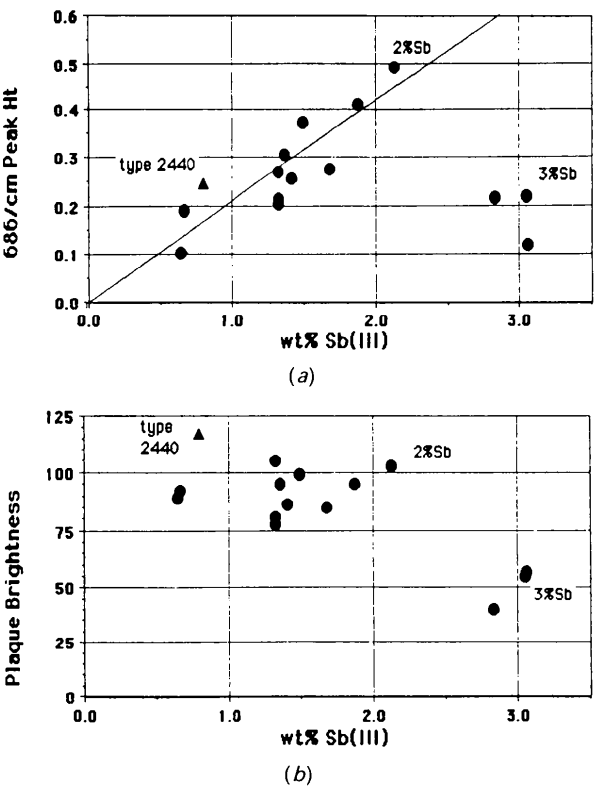

Fig. 1. Measurements on fluorapatite:Sb samples. (*a*) Heights of the 686 cm^{-1} absorbance peak from 2·5 mg samples in KBr pellets *versus* wt% Sb^{III} measured by titration. (*b*) Plaque brightness (arbitrary scale) *versus* wt% Sb^{III}.

The 3%Sb sample contained 3·08 wt% soluble Sb^{3+} (0·264 Sb per unit cell) and only an unweighable trace of acid insoluble material. (These values correspond to firing losses of 41 and 49%, respectively, of the antimony in the initial preparative mixtures. Antimony retention was erratic, reflecting at least the high vapor pressures of the components at 1473 K and variations in the fit of any particular lid and crucible.) The '0%Sb' control fluorapatite sample was prepared from a mixture of the oxide, fluoride, and pyrophosphate formulated to give 9·90 Ca per 6 P and 2 F, and fired as above. [The deficiency in calcium is needed to compensate losses of phosphorus and fluoride in firing (Rabatin & Gillooly, 1965). A simultaneous firing of a 9·95 Ca formulation gave residual CaO.] Each of these samples was ground to pass through a 400 mesh sieve, washed in dilute acid and then deionized water, dried, and resieved.

To be sure that the samples, especially the 2%Sb, were 'the same' as halophosphate phosphors containing lower concentrations of Sb, several other properties of these samples were compared to those of commercial halophosphate phosphors. Emission and excitation spectra of the 2%Sb and 3%Sb samples are compared to those of Sylvania type 2440 in Fig. 2. Table 1 presents the results of elemental analyses for the principal components. All three samples were also examined by spark-source spectrographic analysis. The highest contaminant levels were for strontium and lead, both in the '50–500 p.p.m.' range, or 0·002 to 0·025 times the lesser antimony concentration. Mg, Al and Si were reported in the 10–100 p.p.m. range. The Mossbauer absorption spectrum of the 2%Sb sample (Patton, 1987) has not been analyzed, but is visually highly similar to those of commercial halophosphate phosphor samples superimposed upon that of calcium meta-antimonate. The 3%Sb sample's Mossbauer spectrum (Patton, 1987) shows obvious differences, but with the chemical shift in the same Sb^{3+} region.

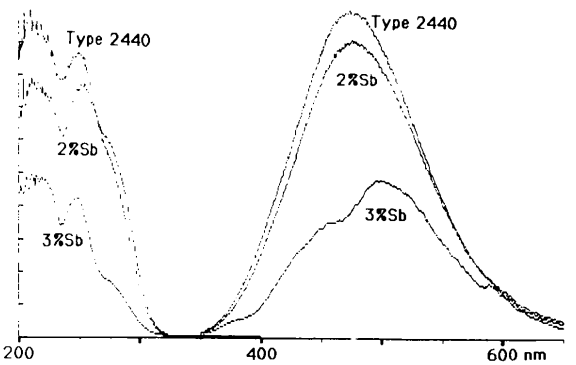

Fig. 2. Emission and excitation spectra of the 2%Sb and 3%Sb samples compared to those of Sylvania type 2440. The excitation spectra (at short wavelength) have been corrected for the instrument response, but the emission spectra have not. The Type 2440 and 2%Sb spectra are on the same scale; those of the 3%Sb are arbitrarily scaled. (The 2440 and 2%Sb excitation curves do cross. The feature near 580 nm in the 3%Sb emission is an instrumental artifact.)

Table 1. *Elemental analyses of samples*

'0%Sb' sample	wt%	Atomic ratios	Ideal ratios
Ca	39·57 (5)[a]	10	10
P (as PO_4)	56·17 (9)	5·990 (12)	6
F	4·40 (5)	2·35 (3)	2
Total	100·1 (1)		

'2%Sb' sample	wt%	Atomic ratios	Rescaled to Ca + Sb = 10
Ca	37·29 (9)	10	9·815
P (as PO_4)	54·55 (9)	6·17 (2)	6·06
F	3·42 (15)	1·94 (9)	1·90
Sb^{3+}	2·14 (2)[b]	0·189 (2)	0·185
$CaSb_2O_6$	2·23 (2)	-	-
Total	99·6 (2)		

'3%Sb' sample	wt%	Atomic ratios	Rescaled to Ca + Sb = 10
Ca	37·44 (11)	10	9·736
P (as PO_4)	55·22 (25)	6·22 (3)	6·06
F	3·65 (8)	2·06 (4)	2·00
Sb^{3+}	3·08 (2)	0·271 (2)	0·264
$CaSb_2O_6$	(trace)	-	-
Total	99·4 (3)		

Notes: (*a*) The appended number in parentheses is the estimated standard deviation in the last digit listed: *e.g.* 12·3 (45) = 12·3 ± 4·5. (*b*) 2·14 wt% Sb^{3+} ÷ (1 − wt fraction $CaSb_2O_6$) = 2·19 wt% in the fluorapatite phase.

Our primary interest is in the 2%Sb sample since it is most similar to the commercial phosphor, but as the 3%Sb was in hand, it was also studied to see if alternate antimony site(s) could be identified. As will be seen, contrasting the two results increases our confidence in each.

3. X-ray diffraction data

Powder X-ray diffraction data were collected at the Georgia Institute of Technology by step-scanning on a locally modified horizontal Siemens θ–2θ diffractometer equipped with a fine-focus copper X-ray tube and a curved graphite diffracted-beam monochromator set for the Cu $K\alpha$ doublet. Because these samples give essentially no reflection-profile broadening, a small, 0·02° 2θ, step size was used. As the success of this experiment would depend critically upon the precision of the data, a counting time of 20 s per step was chosen. Thus, each data collection run required about 34 h for the 5751 steps in the chosen range 15°–130° 2θ. Furthermore, each data set used in the analyses was the sum of two consecutive runs, made without disturbing the sample, and starting at different times of day to reduce the effect of diurnal intensity variations. These systematic diurnal variations were found in preliminary experiments in which one line of a gold standard was repeatedly measured over an extended time period. They have a range of about 2% and are thought to

be due to time-of-day correlated changes in the humidity and/or temperature of the air in the beam paths. The experiment with the gold standard also served to verify the electronic and mechanical stability of the instrument.

The powders were packed into a 16 mm diameter hole in an aluminium disk. These powders had very little cohesiveness, so a few drops of dilute sugar (sucrose) solution were allowed to soak into the packed powder and dry before handling. No diffraction lines due to the sugar were detected in the data sets. These samples have a relatively large crystallite size which gives unacceptable random errors in the diffracted intensities because too few crystallites are in diffracting position to give good averaging (*i.e.* a powder diffraction photograph would show 'grainy' rings) unless special measures are taken. These errors were minimized by continuously rotating the specimen and oscillating the rotation axis by $\pm 1^\circ$. Diffraction patterns so collected were reproducible in detail, whereas those from stationary specimens were not.

Each of the three sample materials had a summed-double-scan data set collected from it as described above. The packed powder was then removed from the aluminium disk, a new diffraction specimen of that material prepared, and another data set collected in the same manner. This gave the six data sets analyzed below.

The precision of the duplicate data sets obtained for each of the samples was examined by comparing them to one another as follows. One feature of the Rietveld refinement program employed (see below) is that it produces a list of the calculated and 'observed' integrated intensities for each *hkl* peak. The 'observed' values are slightly model-dependant in that, for peaks which overlap accidentally or because they are *hkl*, *khl* pairs, the experimental intensity minus background at each 2θ is apportioned in the same ratio as the calculated intensities at that point. The program thus provides a list of *hkl*, I(obs) pairs from each data set. These lists, obtained from the best fits of the models described below, were compressed by summing the α_1 and α_2 components and further summing the *hkl*, *khl* pairs. Standard deviations were set equal to the square root of the sum of the integrated number of counts plus an estimate of the background counts under each peak, and the duplicate data sets from each sample compared. For each of the three pairs of data sets, the distribution of the differences divided by their composite standard deviations was not significantly different from a normal distribution of unit variance. The same was true of subsets restricted to low 2θ angles, and inspection of these Δ/σ plotted against I(obs) or against 2θ showed no noticeable systematic variations. We conclude that *the data sets represent the samples as prepared to the limit imposed by counting statistics.**

4. Results and discussion

In order to obtain the maximum confidence in our results (and most effectively persuade our present readers), the diffraction data were analyzed by both Rietveld refinements and examination of electron density difference maps. Of course, the data remain the same, so the methods are redundant to the degree that they incorporate the same assumptions.

4.1. *Rietveld refinements*, 2%Sb *sample*

Each of the six data sets was used to refine the parameters of a fluorapatite model in which the scale factor and all but one atomic occupancy factor were varied. The atomic positions and pattern parameters (peak widths, cell dimensions, true zero of 2θ, background function, preferred orientation parameter, *etc.*) were also varied, but the individual anisotropic thermal parameters were held fixed at the values found in a precise single-crystal determination (Sudarsanan, Mackie & Young, 1972) and only a single overall isotropic thermal motion parameter varied. These crystal structure refinements were carried out in space group $P6_3/m$ using the Rietveld whole-pattern-fitting structure refinement method (Rietveld, 1969; Wiles & Young, 1981) by means of a recent version of computer program *DBW*3.2, which is an upgraded version of the program described by Wiles & Young (1981). The pseudo-Voigt profile function of Thompson, Cox & Hastings (1987), truncated at five times the width at half-height, was used with an asymmetry correction at low angles and backgrounds were fit by cubic polynomials in 2θ. Preferred orientation effects were fit by a Gaussian function of the angle between the diffraction vector and ± 001 (but we now prefer other forms). Atomic scattering factors used were those listed for Ca^{2+}, neutral P, F^- and O^- in *International Tables for X-ray Crystallography* (1974, Vol. IV), and included anomalous dispersion. The calcium meta-antimonate second phase, whose structure was redetermined for this work (Young, Sakthivel & DeBoer, 1991), was included in the refinements against the 2%Sb data sets with fixed positional, thermal and occupancy

* Lists of the 'observed' integrated peak intensities and of references to the Sb^{III} structures examined for bonding geometry have been deposited with the British Library Document Supply Centre as Supplementary Publication No. SUP 54197 (5 pp.). Copies may be obtained through The Technical Editor, International Union of Crystallography, 5 Abbey Square, Chester CH1 2HU, England. Magnetically recorded copies of three raw data sets have been deposited with the Joint Committee on Powder Diffraction Standards – International Center for Diffraction Data, 1061 Park Lane, Swarthmore, PA 19081, USA.

Table 2. *Final refined crystal and atomic parameters*

Sample		0%Sb		2%Sb		3%Sb	
Data set	FAp[a]	'13	'14	'15	'16	'17	'18
R_{wp}[b] (%)	(2·8)	12·46	12·58	12·88	12·90	12·45	12·47
S_{wp}	–	1·35	1·36	1·38	1·38	1·34	1·35
R_B (%)	1·6	5·04	4·46	7·10	6·61	5·31	5·32
a (Å)	9·367 (1)[c]	9·3692[d]	9·3690	9·3749	9·3750	9·3713	9·3715
c (Å)	6·884 (1)	6·8840	6·8839	6·8903	6·8904	6·8866	6·8867
N(Ca1)	$\frac{1}{3}$	0·3456 (14)	0·3463 (14)	0·3399 (16)	0·3417 (16)	0·3511 (16)	0·3526 (16)
N(Ca2)	$\frac{1}{2}$	0·5166 (18)	0·5164 (18)	0·5271 (23)	0·5317 (23)	0·5340 (22)	0·5386 (22)
N(P)	$\frac{1}{2}$	$\frac{1}{2}$	$\frac{1}{2}$	$\frac{1}{2}$	$\frac{1}{2}$	$\frac{1}{2}$	$\frac{1}{2}$
N(F)	$\frac{1}{6}$	0·1690 (15)	0·1686 (15)	0·1567 (17)	0·1611 (17)	0·1736 (16)	0·1771 (16)
N(O3)[e]	1	1·0475 (31)	1·0452 (31)	1·0273 (37)	1·0406 (36)	1·0696 (36)	1·0817 (36)
$B_{iso,all}$	·	−0·002 (17)	0·044 (17)	−0·144 (20)	−0·193 (20)	−0·143 (19)	−0·112 (19)
z(Ca1)[f]	0·0011 (0)	0·0011 (3)	0·0013 (3)	0·0019 (4)	0·0015 (4)	0·0020 (4)	0·0018 (4)
x(Ca2)	0·2416 (0)	0·2417 (2)	0·2417 (2)	0·2398 (2)	0·2397 (2)	0·2410 (2)	0·2413 (2)
y(Ca2)	−0·0071 (0)	−0·0073 (2)	−0·0074 (2)	−0·0060 (2)	−0·0064 (2)	−0·0079 (2)	−0·0074 (2)
x(P)	0·3981 (0)	0·3980 (2)	0·3978 (2)	0·3993 (3)	0·3996 (3)	0·3973 (2)	0·3971 (2)
y(P)	0·3688 (0)	0·3684 (2)	0·3685 (2)	0·3698 (2)	0·3697 (2)	0·3684 (2)	0·3682 (2)
x(O1)	0·3262 (1)	0·3264 (5)	0·3264 (5)	0·3256 (5)	0·3259 (5)	0·3270 (5)	0·3271 (5)
y(O1)	0·4843 (1)	0·4859 (5)	0·4859 (5)	0·4855 (5)	0·4849 (5)	0·4865 (5)	0·4873 (5)
x(O2)	0·5880 (1)	0·5890 (5)	0·5890 (5)	0·5881 (6)	0·5876 (5)	0·5886 (5)	0·5887 (5)
y(O2)	0·4668 (1)	0·4669 (5)	0·4669 (5)	0·4655 (6)	0·4651 (5)	0·4672 (5)	0·4670 (5)
x(O3)	0·3416 (1)	0·3421 (4)	0·3421 (4)	0·3438 (5)	0·3437 (4)	0·3378 (4)	0·3384 (4)
y(O3)	0·2568 (1)	0·2575 (4)	0·2575 (4)	0·2572 (4)	0·2568 (4)	0·2550 (4)	0·2558 (4)
z(O3)	0·0704 (1)	0·0705 (4)	0·0705 (4)	0·0680 (5)	0·0677 (5)	0·0713 (4)	0·0712 (4)

Notes: (*a*) Sudarsanan, Mackie & Young (1972). (*b*) Agreement measures listed are $R_{wp} = \{\sum_i[(yo_i - yc_i)/\sigma(yo_i)]^2/\sum_i[yo_i/\sigma(yo_i)]^2\}^{1/2}$; $S_{wp} = R_{wp}/R_{ex}$, where $R_{ex} = \{[(\sum_i 1) - p]/\sum_i[yo_i/\sigma(yo_i)]^2\}^{1/2}$; and $R_B = \sum_k|Io_k - Ic_k|/\sum_k Io_k$. yo_i and yc_i are the observed and calculated intensities at the ith 2θ step, p is the number of parameters varied, and Io_k, Ic_k are the observed and calculated peak areas under the kth diffraction peak. See the text, Rietveld (1969) and Wiles & Young (1981). (*c*) Estimated standard deviations are represented as in Table 1. (*d*) Standard deviations of unit-cell dimensions resulting from the refinements are unrealistically small (0·00005 Å) for reasons mentioned in text and in Hill & Madsen (1986). (*e*) Occupancy factors (N) of O1 and O2 were constrained to be one-half that of O3. (*f*) Symmetry-fixed coordinates not listed are: x, y of Ca1 = $\frac{1}{3}$, $\frac{2}{3}$; x, y, z of F = 0, 0, $\frac{1}{4}$; and z of Ca2, P, O1 and O2 all = $\frac{1}{4}$. All refinements were carried out in space group $P6_3/m$.

parameters, but variable scale factor, cell dimensions, peak widths and preferred orientation. A selection of the final refined parameters are compared to one another [and to those of Sudarsanan, Mackie & Young (1972), labelled 'FAp'] in Table 2. We point out the excellent agreement between results from duplicate data sets on the same sample and the small S_{wp} ($= R_{wp}/R_{ex}$) values. The typical agreement obtained is illustrated in Fig. 3.

As is apparent in Table 2, the occupancy factors, N, of the three oxygen atoms were constrained to represent equal multipliers on the ideal values, and that of phosphorus held fixed. One linear combination of the scale factor and the set of all the occupancy factors must be held fixed in the least-squares refinement process, since they form a linearly dependent set and would otherwise give a singular least-squares matrix. In the absence of a measurement of the absolute magnitudes of the X-ray scattering, only relative occupancies can be determined, and a further ambiguity is introduced by the unknown differences between the atoms' actual scattering factors (electron distributions) in the chemical compound *versus* those calculated for isolated atoms and used in the

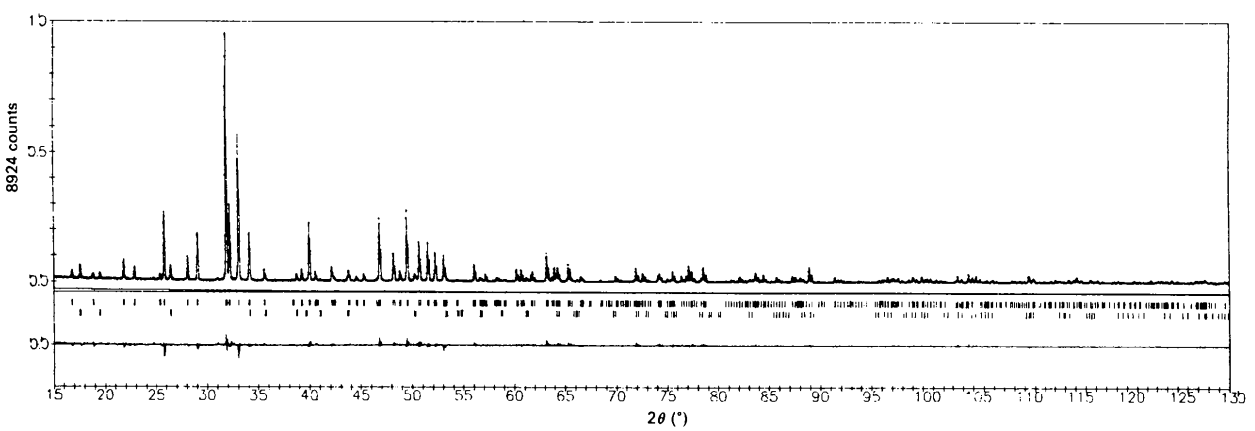

Fig. 3. Typical agreement found in the Rietveld refinements, illustrated for the 2%Sb sample. The upper curve dots are the observed data and the overlying line is the calculated fit. The lowest curve shows the differences. Vertical lines mark the positions of all Bragg reflections in this range for the apatite (upper set) and for the meta-antimonate (lower set).

Table 3. *Relative occupancy factors and their ratios between samples*

Sample/data	Ca2/Ca1	P/Ca1	F/Ca1	O's/Ca1
Ideal	1·5	1·5	0·5	3·0
0%Sb/'13	1·495 (5)	1·447 (6)	0·489 (5)	3·031 (9)
0%Sb/'14	1·491 (5)	1·444 (6)	0·487 (5)	3·018 (9)
2%Sb/'15	1·551 (6)	1·471 (7)	0·461 (5)	3·022 (11)
2%Sb/'16	1·556 (6)	1·463 (7)	0·471 (5)	3·045 (11)
2%/0% ratio	1·040 (5)	1·015 (6)	0·955 (14)	1·003 (5)
Deviation	$+8{\cdot}0\sigma$	$+2{\cdot}5\sigma$	$-3{\cdot}2\sigma$	$+0{\cdot}6\sigma$
3%Sb/'17	1·521 (6)	1·424 (6)	0·494 (5)	3·046 (10)
3%Sb/'18	1·528 (6)	1·418 (6)	0·502 (5)	3·068 (10)
3%/0% ratio	1·021 (5)	0·983 (6)	1·020 (14)	1·011 (4)
Deviation	$+4{\cdot}2\sigma$	$-2{\cdot}8\sigma$	$+1{\cdot}4\sigma$	$+2{\cdot}5\sigma$

refinement program. Therefore, these relative occupancies may be rescaled to any convenient basis. Table 3 shows the occupancy factors rescaled to Ca(1) and the ratios of these for the Sb substituted samples relative to the 0%Sb sample, together with the standard deviations as calculated using both the correlation coefficients and the individual standard deviations resulting from the inverses of the final least-squares matrices. (The correlation coefficients among the occupancy factors were all positive, ranged from 0·15 to 0·68, and were found to have the same values, $\pm 0{\cdot}01$, in all six final refinement cycles.) This comparison shows that the 2%Sb sample has eight combined standard deviations of excess electron density at the Ca(2) site and a deficiency of $3{\cdot}2\sigma$ at the ideal fluoride site, the other sites not differing significantly from equality. *We regard this as strong evidence that antimony substitutes into the* Ca(2) *site*, and a suggestion that a missing or displaced fluoride is associated with that substitution.

No consistent interpretation could be found for the refined occupancies of the 3%Sb sample, which showed a smaller excess at Ca(2) and relative deficiencies at both Ca(1) and P. The reason for this became apparent when electron density difference maps were calculated and examined.

4.2. *Precision of the Rietveld refinement results*

Several authors (Hill & Madsen, 1986, and references therein) have argued that the Rietveld refinement method systematically underestimates standard deviations. Others disagree (*e.g.* Prince, 1981, 1985) and we point out the consistency between our results from duplicate data sets, between the duplicated data sets themselves (shown above) and the agreement of the 0%Sb positional parameters with those of Sudarsanan, Mackie & Young (1972). Furthermore, in no case of which we are aware has more than a factor of two misestimation been claimed for structural parameters. (Cell-dimension e.s.d.'s are frequently much worse, since they depend on the positions, not the intensities, of the peaks, and these are subject to highly nonrandom errors.) However, even if the standard deviations of the relative occupancies are arbitrarily doubled, our principal conclusion remains.

The meaning of substitution 'at' a given site is limited by the resolution of the data. Two locations in the crystal separated by less than about half the wavelength of the highest Fourier component measured cannot be resolved. For the present $\lambda/2\sin(\theta_{max}) = 0{\cdot}834$ Å, two locations separated by less than about 0·4 Å would not be seen as different. Our present actual situation gives substantially less resolution, because the detectability of the differences due to antimony substitution declines to less than one standard deviation in the data at diffraction angles of only about 80° 2θ, corresponding to a resolution of about 0·6 Å. At first, it seems incorrect that the 'signal' should decrease with diffraction angle, since antimony is a heavier atom whose greater core electron density gives relatively more scattering at higher angles. Calculation shows that the fractional antimony contribution to the scattering does indeed increase with angle, but not fast enough to overcome the worsening relative precision of the measured intensities as those intensities become weaker at higher angles. The large $\Delta I/\sigma(I)$ values are indeed found to be concentrated at the smaller diffraction angles.

4.3. *Electron density methods*, 2%Sb *sample*

For our present purposes, the least-squares Rietveld refinement method suffers from a conceptual defect in that it 'tests for' the presence of the increased scattering power of the substituted antimony only at, and near, the sites of the atoms composing the host crystal and not at interstitial sites. Therefore, a second method of analysis which is not so constrained was also used.

The changes in the diffracted intensities between the antimony substituted and unsubstituted samples contain the information about the changes in the averaged electron density distribution caused by the antimony substitution. Since the host crystal is centrosymmetric, the phases of the scattered-amplitude differences are unambiguous. We calculate the Fourier inverse of the structure-factor differences between the samples (*i.e. observed* x%Sb minus 0%Sb differences, as opposed to the more common observed minus model differences) and expect to see positive electron density at the antimony position. Negative density is expected at positions (if any) caused to be vacated by antimony insertion. An error in the scaling between the two observed data sets will appear as an added positive or negative image of the entire host structure (Fig. 4).

The data sets for this procedure were the 'observed' integrated intensities produced by the

Rietveld refinement program, as described in the final paragraph of §3, above. All four 'I_{obs}' values (the $K\alpha_1$ and $K\alpha_2$ components from each of the two separate diffraction data sets) were summed for each Bragg peak up to $2\theta = 80°$ of the 0%Sb sample and of the 2%Sb sample. Contributions of superimposed inequivalent *hkl* and *khl* diffractions were included in a single peak's intensity. Counting-statistics standard deviations including the background contributions were calculated and the two sets of integrated intensities were scaled anisotropically to account for differences in preferred orientation that had been found in the diffraction samples. The scale factor between corresponding intensities was $(s_1\sin^2\varphi + s_2\cos^2\varphi)$, where s_1 and s_2 were adjusted by hand for the minimum $\sum[\Delta(I_{obs})/\sigma(\Delta I_{obs})]^2$ and φ is the angle between the reciprocal lattice vector and c^*. The best fit s_1/s_2 ratio was 1·73 and no visible trends remained in plots of $\Delta I/\sigma$ against φ or 2θ.

The signed amplitudes for the observed-differences electron density map were calculated from the scaled intensities as:

$$\Delta F = F_{calc}(0\%Sb) \times \{\sqrt{[I(2\%Sb)/I(0\%Sb)]} - 1\}.$$

This divides the intensity change between the pairs of *hkl* and *khl* Fourier terms in proportion to their calculated $|F|$'s (as opposed to, say, equally or proportional to F^2).

This gave 119 Fourier terms from the 83 diffraction peaks in the 15–80° 2θ range. The 100 diffraction occurs below 15°, and the 220 term was omitted because its calculated F was too small to give reliable phasing. Sections were calculated in increments of $\frac{1}{16}$ from $z = 0$ to $z = \frac{1}{4}$, but significant features occur only in the $z = \frac{1}{4}$ section. This part of the observed-differences electron density map is shown in Fig. 5.

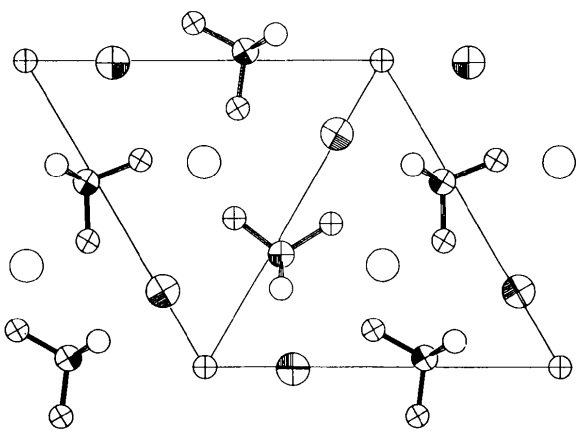

Fig. 4. A section centered at the $z = 0·25$ mirror plane of the calcium fluorapatite structure. A filled octant marks the Ca(2) and phosphorus atoms, a cross, the fluorine and in-plane oxygens, and plain circles, the out-of-plane Ca(1) and O(3) atoms. Compare with Figs. 5 and 6.

[The maximum difference density may be compared to the values of 27·8 and 27·3 e Å^{-3} calculated for Ca(2) and Ca(1), respectively, using the F_{calc}(0%Sb) for the same set of *hkl*'s. This theoretical density function was calculated to verify the correctness of the *ad hoc* programs used and to observe the effects of data set truncation.]

In order to assess the statistical significance of the electron densities, their standard deviations were also calculated by propagating the standard deviations of the intensities through the calculation of ΔF and the Fourier inversion. The standard deviation of the difference density, $\sigma(\rho)$, ranges from 0·05 to 0·59 e Å^{-3} and shows broad maxima at all integer multiples of $\frac{1}{6}, \frac{1}{3}, z$ (including $\frac{1}{3}, \frac{1}{6}, z$; 0, $\frac{1}{2}, z$; *etc.*) for all values of z. The maxima vary slightly in a pattern that necessarily conforms to $P6/m$ with a halved c axis. (The correlation between symmetry-related Fourier terms prevents halving the a and b axes, but the function very nearly fits this symmetry as well.) The same function calculated for the 3%Sb minus 0%Sb differences is virtually identical, since the $\sigma(I)$'s are.

The largest difference-density peak is 1·27 e Å^{-3} high and effectively coincident with the Ca(2) site. The exact peak is only 0·20 Å from the refined Ca(2) position listed in Table 2, and its height is 5·4 times the standard deviation calculated at that point. Because of the rapid variation of the standard deviation of the difference density, the $\rho/\sigma(\rho)$ ratio reaches its maximum of 8·6 (= 0·81/0·094) at a position 0·4 Å from the density maximum and 0·6 Å from the Ca(2) position. Other features visible in Fig. 5, at 0, 0, $\frac{1}{4}$ and $\frac{1}{3}, \frac{2}{3}, \frac{1}{4}$, are not significant, each being less than 0·8 of the standard deviation calculated for that point.

The conclusion that the antimony occupies the Ca(2) site in this fluorapatite sample is strongly confirmed by this result.

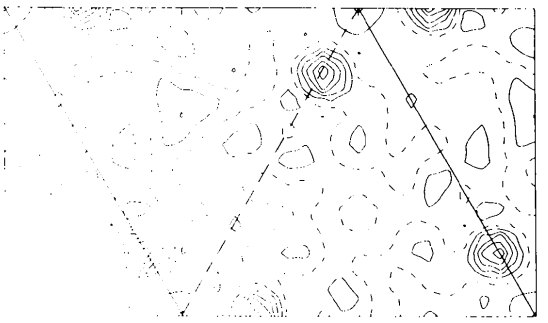

Fig. 5. Contour map of the observed-differences electron density at $z = 0·25$ for the 2%Sb sample. Contours are drawn at intervals of 0·2 e Å^{-3} with the zero contour dashed. Deviations from exact symmetry are an artifact of the plotting program used.

4.4. *Electron density methods*, 3%Sb *sample*

The 3%Sb sample, described above, is known to be anomalous as shown by Fig. 1. The Rietveld refinements of atomic occupancy factors gave ambiguous results. Since the 'observed differences' electron density difference map calculation described above 'looks everywhere' in the crystal, not only at (and near) the atomic sites, it was also applied to the 3%Sb diffraction data sets.

The treatment was exactly as described for the 2%Sb case (s_1/s_2 ratio = 1·66), but now the only substantial difference electron density peaks found were at the inequivalent ($\frac{1}{3}$, $\frac{2}{3}$, $\frac{1}{4}$) and ($\frac{2}{3}$, $\frac{1}{3}$, $\frac{1}{4}$) positions, with peak densities of 1·41 and 1·22 e Å^{-3}, respectively, shown in Fig. 6. These densities are 3·43 and 2·95 times the calculated standard deviation of the difference density at these points. These are the 3/*m* Wyckoff 2(*c*) and 2(*d*) positions, on the threefold axis halfway between Ca(1) sites. There are no atoms in these positions in the pure fluorapatite structure. Antimony substitution in these positions would necessarily displace both adjacent Ca(1) ions, as they are only about $c/4 = 1{\cdot}72$ Å distant. The nearest phosphate oxygens are in the $z = \frac{1}{4}$ mirror plane, at 1·68 and 1·74 Å, respectively. One could speculate that rotation of the PO_4 groups and some displacement could achieve more typical Sb—O distances of about 1·95 Å. Charge balance and a reason for both positions to be occupied are achieved if we suppose that three adjacent Ca(1) ions are replaced by two adjacent Sb^{3+}.

We might have expected that the observed-differences electron density maps from the 3%Sb data would also show the peak at the Ca(2) position, from the expectation that, as the antimony concentration is increased above a saturation level for one site, an additional site would also begin to be occupied, rather than that the first site would be entirely emptied, as appears (within our modest precision) to have occurred in the 3%Sb sample. This seems especially true for a change between such low concentrations that the 2%Sb sample contains only one Sb in 5·4 unit cells, and the 3%Sb, one in 3·8 unit cells, each containing $Ca_{10}(PO_4)_6F_2$. However, the absence of a peak at the Ca(2) site in the 3%Sb minus 0%Sb density difference does argue strongly against any speculation that the peak found in the 2%Sb case could have been due to a 'hole' (Ca deficiency) in the 0%Sb standard rather than a 'peak' (Sb substitution) in the 2%Sb sample.

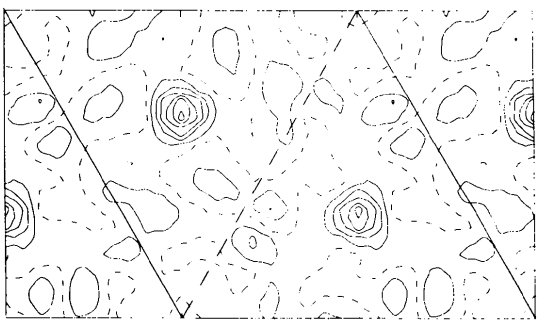

Fig. 6. Contour map of the observed-differences electron density at $z = 0{\cdot}25$ for the 3%Sb sample. Conditions as in Fig. 5.

4.5. *Rietveld refinement*, 3%Sb *sample*

With the indication from the observed-differences density maps as above, two fractional antimony atoms were added to the Wyckoff 2(*c*) and 2(*d*) positions of the Rietveld refinement models of the 3%Sb samples previously refined. No significant improvement in agreement was found in continued refinements with either individual occupancy parameters and fixed isotropic thermal parameters, or with both occupancy and thermal parameters allowed to vary. In the former case, the occupancies converged to 0·0010 (3) and 0·0004 (3), and in the latter, 0·0012 (5) and 0·0006 (4). At least in this case, it appears that comparison of two models least-squares fit to two data sets cannot 'see' differences as well as the electron density difference map comparison.

5. Some caveats and rebuttal

Strictly speaking, what these experiments and data analyses have demonstrated is increased electron density at certain crystallographic sites of the 2%Sb and 3%Sb samples relative to the 0%Sb standard, and we then infer that these are the antimony substitution sites. This experiment is not sensitive enough to exclude small amounts of antimony substitution at other sites in addition to those reported above. We roughly estimate that the amount of such second site substitution that could have escaped notice would not be greater than about one quarter of what was found, and our diffraction results are entirely consistent with zero populations at other sites. Of course, the 3%Sb sample's non-zero luminescence and 686 cm^{-1} absorption indicate that it has some small amount of antimony in the Ca(2) site.

A suggestion that the electron density increase at Ca(2) in the 2%Sb sample might be due to missing Ca atoms (defects) in the 0%Sb standard is untenable because: (*a*) We do not see a peak in that location in the 3%Sb minus 0%Sb difference map. (*b*) All three samples were synthesized under as nearly as practicable the same conditions. (*c*) The density of calcium defects would have to be so high that the antimony contribution, which is still present, is lost in the 'noise' in comparison. [If we assume a true, but buried in the noise, antimony peak one-quarter as large as the supposed missing-calcium

peak and a ratio of Sb:Ca scattering strengths of only 2:1 (< 51/20), we would require $4 \times 2 \times 0{\cdot}185 = 1{\cdot}5$ missing Ca (and missing anions to balance charge) per cell of $Ca_{10}(PO_4)_6F_2$. All of the fluoride in the unit cell is insufficient to provide the charge balance, and if we assume one PO_4^{3+} is missing, about 15% of the cell volume (using cubes of the ionic radii, neglecting P) of the antimony-free standard would have to be empty space. The density would also be reduced by 15%. This while the antimony-doped sample has no such defects and the difference map also fails to show a peak for the missing phosphate group.]

The chemical analysis in Table 1 does show a high fluoride content for the 0%Sb sample, but the Ca/P ratio is not perturbed, *i.e.* the excess fluoride appears to have no counter ion. One could imagine $Ca_{10}(PO_4)_{6-x}(FPO_3)_xF_{2+x}$, where the monofluorophosphate would rapidly hydrolyze during the analysis, but that anion is not seen in the infrared spectrum. We have no satisfactory explanation for the fluoride analysis, but see no way in which it contradicts our diffraction results.

The Beer's law slope of the plot of 686 cm^{-1} peak heights against titrated Sb^{III} content, Fig. 1, is less steep than that found for a set of samples prepared by colleagues some years ago (Dale, 1987). However, these were prepared from different starting materials, under a different atmosphere, in different equipment, and at a lower temperature. If the slope difference is taken as evidence of substitution in two sites, they would be roughly equally populated and we should have seen both sites in the diffraction results. It would be consistent to suppose that there are two or more different antimony nearest-neighbor environments all of which are on the same crystallographic site, but only some of which contribute to the 686 cm^{-1} peak. Combining the data of Fig. 1(*a*) with recent ^{19}F solid-state NMR observations (Moran, Yesinowski, & Berkowitz, 1991) indicates the presence of more than one antimony environment (about 75% giving the 686 cm^{-1} peak in the 2%Sb sample) and 'explains' the scatter in Fig. 1(*a*).

6. Local environment of Sb in fluorapatite

That Sb^{III} has a stereochemically active lone pair of electrons that occupy approximately the volume of an additional oxygen ligand, and is *not* a spherical ion, appears to have gone unconsidered in nearly all previous discussions of the environment of antimony in apatites [exceptions are Mishra, Patton, Dale & Das (1987) and Oomen, Smit & Blasse (1988)]. Seventy-nine crystal structure reports from the Inorganic Crystal Structure Database (from the Fachinformationszentrum Karlsruhe, Germany) (Bergerhoff, Hundt, Sievers & Brown, 1983) for substances containing Sb^{III} and F, O, or S were first selected for reliability of the structure report and nonduplication of composition and polymorph. (The ICSD collection code numbers, formulas and CODEN references are listed in the deposited materials.) Then, the distances and angles of the ligands on antimony in each of these were examined. Antimony(III) was invariably found to have a single-sided coordination, that is, all atoms bound to antimony(III) occupied a common hemisphere. (Two apparent exceptions were obviously due to multiple disorder on high-symmetry sites.) Antimony(III) was found in 3, 4 and 5 coordination and the coordinating atoms included F, O, S, mixed F and O, and mixed O and S. Oxygen ligands included those bound in phosphate, sulfate, nitrate and other oxyanions. We conclude that any plausible model for Sb^{III} in apatites must exhibit a similar one-sided array of ligands due to the presence of the lone pair.

The approximate invariance of the antimony emission and excitation spectra with changes in the identity of the halide has been taken as supporting the oxygen-for-halide substitution of the Ouweltjes (1952) model. This is inconsistent with the apparently decreased electron density we find at the fluoride ion site in the 2%Sb sample. We may speculate that if the antimony lone pair occupies the adjacent halide site this would account for both observations (but does not provide for charge compensation).

We are unable, at this time, to offer any complete detailed model for the near-neighbor environment(s) of antimony in either the 2%Sb or 3%Sb sample. The Mossbauer evidence indicates that something quite similar to the $:SbO_3^{3-}$ model of Mishra, Patton, Dale & Das (1987) will be needed for phosphors and our 2%Sb sample, but our results require it at the Ca(2) site instead of substituted for PO_4^{3-}. Attempts to reconcile all available evidence and derive consistent models continue.

We gratefully acknowledge the good advice of G. Gillooly on methods of forming high antimony content fluorapatite. We thank P. Suitch and S. Fisher for technical assistance. J. Saunders, J. Greene and R. Fowler are thanked for infrared spectra, elemental analyses and advice on the Sb^{III} titration, respectively. E. Dale, K. Mishra, J. Berkowitz, R. Patton and C. Lagos are all thanked for useful information and helpful, if sometimes vigorous, discussions.

References

BERGERHOFF, G., HUNDT, R., SIEVERS, R. & BROWN, I. D. (1983). *J. Chem. Inf. Comput. Sci.* **23**, 66–69.

DALE, E. A. (1987). Personal communication.

DAVIS, T. S., KREIDLER, E. R., PARODI, J. A. & SOULES, T. F. (1971). *J. Lumin.* **4**, 48–62, especially footnote 21.

GILLOOLY, G. R. (1971). Ext. Abstr. 139th Nat. Meet. Electrochem. Soc., Abstract No. 40, pp. 111–113.
HILL, R. J. & MADSEN, I. C. (1986). *J. Appl. Cryst.* **19**, 10–18, and references therein.
MISHRA, K. C., PATTON, R. J., DALE, E. A. & DAS, T. P. (1987). *Phys. Rev. B*, **35**, 1512–1520.
MITSUISHI, T. & EMOTO, M. (1967). *Hitachi Rev.* **16**, 230–235.
MORAN, L. B., YESINOWSKI, J. P. & BERKOWITZ, J. K. (1991). In preparation.
OOMEN, E. W. J. L., SMIT, W. M. A. & BLASSE, G. (1988). *Mater. Chem. Phys.* **19**, 357–368.
OUWELTJES, J. (1952). *Philips Tech. Rev.* **13**, 346–351.
PATTON, R. (1987). Personal communcation.
PRINCE, E. (1981). *J. Appl. Cryst.* **14**, 157–159.
PRINCE, E. (1985). *Structure and Statistics in Crystallography*, edited by A. J. C. WILSON, pp. 95–103. Guilderland, NY: Adenine Press.
RABATIN, J. G. & GILLOOLY, G. R. (1965). *J. Electrochem. Soc.* **112**, 489–492.
RABATIN, J. G., GILLOOLY, G. R. & HUNTER, J. W. (1967). *J. Electrochem. Soc.* **114**, 956–959.
RIETVELD, H. M. (1969). *J. Appl. Cryst.* **2**, 65–71.
SOULES, T. F., DAVIS, T. S. & KREIDLER, E. R. (1971). *J. Chem. Phys.* **55**, 1056–1064.
SUDARSANAN, K., MACKIE, P. E. & YOUNG, R. A. (1972). *Mater. Res. Bull.* **7**, 1331–1337.
THOMPSON, P., COX, D. E. & HASTINGS, J. B. (1987). *J. Appl. Cryst.* **20**, 79–83.
WARREN, R. W., RYAN, F. M., HOPKINS, R. H. & VANBROEKHOVEN, J. (1975). *J. Electrochem. Soc.* **122**, 752–760.
WILES, D. B. & YOUNG, R. A. (1981). *J. Appl. Cryst.* **14**, 149–151.
YOUNG, R. A. (1988). *Aust. J. Phys.* **41**, 297–310.
YOUNG, R. A., DEBOER, B. G., SAKTHIVEL, A. & CAGLE, J. R. (1988). 11th Eur. Crystallogr. Meet., Vienna, Austria, 28 August–2 September 1988.
YOUNG, R. A., SAKTHIVEL, A. & DEBOER, B. G. (1991). In preparation.

Acta Cryst. (1991). B**47**, 692–696

Tetragonal Ferroelastic/Antiferroelectric Chromium–Chlorine Boracite, $Cr_3B_7O_{13}Cl$, from X-ray Diffraction on a Single-Domain Crystal at 230 K

BY S. Y. MAO, F. KUBEL AND H. SCHMID

Département de Chimie Minérale, Analytique et Appliquée, Université de Genève, CH-1211 Genève 4, Switzerland

AND K. YVON

Laboratoire de Cristallographie aux Rayons X, Université de Genève, CH-1211 Genève 4, Switzerland

(*Received* 16 *January* 1991; *accepted* 2 *April* 1991)

Abstract

$Cr_3B_7O_{13}Cl$, $M_r = 475{\cdot}12$, tetragonal, $P\bar{4}2_1c$ (114), $a = 12{\cdot}1410\ (3)$, $c = 12{\cdot}1606\ (4)$ Å, $V = 1792{\cdot}52\ (9)$ Å^3, $Z = 8$, $D_x = 3{\cdot}521$ mg mm^{-3}, λ(Mo $K\alpha$) = 0·71069 Å, μ(Mo $K\alpha$) = 3·393 mm^{-1}, $F(000) = 1824$, $T = 230$ K, $R = 0{\cdot}029$, $wR = 0{\cdot}024$ for 1991 unique reflections. The structure contains five symmetry-independent Cr sites, four with sixfold (4O + 2Cl) and one with fivefold (4O + 1Cl) coordination.

Introduction

$Cr_3B_7O_{13}Cl$ (hereafter Cr-Cl) belongs to the class of fully ferroelectric/fully ferroelastic [nomenclature of Aizu (1970)] $M_3B_7O_{13}X$ boracites, where M denotes a divalent metal ion and X a halogen ion. The optic, dielectric and pyroelectric properties of Cr-Cl have been studied by various authors (Nesterova, Pisarev & Andreeva, 1974; Bochkov & Drozhdin, 1975; Schmid & Tippmann, 1978). At room temperature Cr-Cl has cubic symmetry and space group $F\bar{4}3c$ (Nelmes & Thornley, 1974). Upon decreasing the temperature it undergoes two structural phase transitions, one at $T_1 = 264$ K to a tetragonal ferroelastic/antiferroelectric modification of symmetry $\bar{4}2m$, and another at $T_2 = 160$ K to an orthorhombic fully ferroelectric/fully ferroelastic modification of symmetry $mm2$ (Ye, Rivera & Schmid, 1990, 1991*a*):

$$\bar{4}3m \xleftrightarrow{T_1 = 264\ \text{K}} \bar{4}2m \xleftrightarrow{T_2 = 160\ \text{K}} mm2$$

Structural data for the two low-temperature modifications are not yet available. Here we report the single-crystal data of the tetragonal modification. It is the first tetragonal boracite structure to be characterized.

Experimental

Crystals were grown by the chemical vapour transport method (Schmid, 1965; Schmid & Tippmann, 1979). A rectangular parallelepiped single-crystal platelet delimited by cubic (100), (010) and (001) faces (dimensions 0·212 × 0·550 × 0·025 mm) was

0108-7681/91/050692-05$03.00